CHALMERS
UNIVERSITY OF TECHNOLOGY

A grid-based methodology for the assessment of time-dependent building damage at large scale

Tunnelling and Underground Space Technology 149 (2024) 105788

Contents lists available at ScienceDirect

Tunnelling and Underground Space Technology incorporating Trenchless Technology Research

journal homepage: www.elsevier.com/locate/tust

A grid-based methodology for the assessment of time-dependent building damage at large scale

Pierre Wikby [a,*], Ezra Haaf [a], Ayman Abed [a], Lars Rosén [a], Jonas Sundell [a,b], Minna Karstunen [a]

[a] Department of Architecture and Civil Engineering, Chalmers University of Technology, SE-412 96 Gothenburg, Sweden
[b] Swedish Geotechnical Institute, SE-412 96 Gothenburg, Sweden

ARTICLE INFO

Keywords:
Building damage
Differential settlements
Time-dependent settlements
District scale analyses

ABSTRACT

Leakage into underground constructions can result in time-dependent settlements in soft clays. In urban areas with spatial variability in geologic stratification, groundwater conditions and soil compressibility, differential settlements may occur, causing damage to buildings. Current methods for damage assessment that rely on 1D formulations for settlement prediction are not representative for drawdown-induced settlements in heterogeneous environments. Thus, in this paper, we propose a stand-alone approach to integrating spatially distributed, non-Gaussian settlement data into early-stage building damage assessments at a district scale. Deformations computed using a 2D coupled hydro-mechanical finite element model with an advanced constitutive model were then employed to get the time-dependent settlements computed as a 3D grid (along x- and y-directions) over a large area. Building damage was then calculated from these green-field simulations with typically used damage parameters for each building-specific settlement profile and comparing these with damage criteria. The approach was applied to 215 buildings in central Gothenburg, Sweden by simulating scenarios of 10 kPa and 40 kPa pore pressure drawdown in the lower (confined) aquifer. Several scenarios were studied, and the correlation between damage parameters and damage criteria was assessed. Finally, a sensitivity study on grid resolution was performed, as well as a validation against observed damage data. The proposed methodology offers an effective way for early-stage damage assessments at a large area for non-Gaussian settlements so that further investigations and mitigation measures can be targeted to the buildings and locations at the highest risk for damage.

1. Introduction

Underground construction in saturated soil or rock may result in leakage of groundwater, causing changes in the piezometric heads, and consequently time-dependent subsidence in areas with soft clay deposits. This poses a serious threat to the value, function, and stability of buildings in the area of influence of the drawdown, often extending several hundreds of meters away from the site (Burbey, 2002; Langford et al., 2016). During the planning and construction phases, the future consequences of changes in the piezometric head must be evaluated. To accurately assess the impact of a pore pressure drop on buildings, first, the settlements need to be estimated, and second, each building in the impacted area must be assessed using relevant damage parameters and damage criteria. Moreover, the time-dependent aspect of settlements in damage assessments is necessary to account for when planning mitigation measures during construction activities (Merisalu et al., 2023; Sundell et al., 2019) and in the long term.

The current methods for linking settlement predictions with building damage for multiple buildings in an area of influence rely on plausible over-simplifications either in the settlement analyses or in the building damage assessments. Most often surface settlements caused by soft soil tunnelling, deep excavations and mining are represented as Gaussian curves with the maximum settlement at/close to the tunnel/excavation location, e.g. Hsieh and Ou (1998). For leakage-induced settlements, empirical relationships between pore pressure reduction and distance to excavation were proposed by Langford et al. (2016) and were used for estimating the long-term settlements in Piciullo et al. (2021). However, due to the variability in soil depth, groundwater conditions, soil compressibility and creep rate in the impacted area, such empirical estimations are rather crude. Appropriate greenfield settlement predictions must consider the spatial variations of the subsurface as was shown by e.g. Peduto et al. (2021). This can be done e.g. through using

* Corresponding author.
E-mail addresses: pierre.wikby@chalmers.se (P. Wikby), ezra.haaf@chalmers.se (E. Haaf), ayman.abed@chalmers.se (A. Abed), lars.rosen@chalmers.se (L. Rosén), jonas.sundell@sgi.se (J. Sundell), minna.karstunen@chalmers.se (M. Karstunen).

https://doi.org/10.1016/j.tust.2024.105788
Received 17 April 2023; Received in revised form 24 April 2024; Accepted 1 May 2024
Available online 8 May 2024

multi-dimensional numerical models. Such models compute the settlements in nodes often organized as grids on the ground surface, e.g. (Mahmoudpour et al., 2016; Shen and Xu, 2011; Sundell et al., 2019; Teatini et al., 2006; Ye et al., 2016). However, even though the total settlements can cause direct problems, e.g. through increased load to end-bearing piles (Broms et al., 1977), the use of total settlements as a damage criterion does not always accurately correlate to the observed deformations in buildings, as the settlements are often non-uniform across the base of buildings (Burland and Wroth, 1974; Grant et al., 1974).

To address the damage caused by differential settlements, empirical and semi-empirical methods are extensively used, considering e.g. angular distortion, deflection ratio and horizontal strain (Boscardin and Cording, 1989; Burland and Wroth, 1974; Polshin and Tokar, 1957; Skempton and MacDonald, 1956). These methods directly link settlements to the onset of cracking on the building. Building damage parameters can be calculated along the ground surface settlement profiles, e.g., Burland and Wroth (1974), which for non-Gaussian settlements, however, is not trivial.

Various methods have been proposed for assessing settlement profiles using ongoing background settlements i.e. InSAR (Drougkas et al., 2020; Giardina et al., 2019; Peduto et al., 2019; Peduto et al., 2017). Peduto et al. (2017) investigated the maximum total and differential settlements of a building at high resolution through geospatial interpolation of measured InSAR points onto a grid. Peduto et al. (2019) interpolated settlement results across the walls of buildings to yield a realistic profile for the longest outer walls. From these results, various damage parameters were calculated based on the settlement profiles. Drougkas et al. (2020) developed a method for determining damage to buildings at a country scale based on InSAR data. However, as far as the authors are concerned, there is currently no method to calculate future damage from predicted grid-type non-Gaussian settlements with relatively high resolution in changing pore pressure regimes in areas with ongoing background settlements. Hence, we propose a novel method which analyses different building damage criteria using time-dependent 3D grid-type settlement prediction data, not only considering consolidation but also the background creep, which will be accelerated due to changes in the pore pressures. The methodology was applied to a case study, related to a tunnel project in Gothenburg, Sweden, with 215 buildings assessed, covering a large influence area.

2. Methodology

2.1. General strategy

This paper proposes a method for converting 3D settlement data corresponding to a given time into early-stage 2D damage assessments. This approach is similar to the first stage of the three-stage approach proposed for Gaussian settlements by Mair et al. (1996). The damage parameters were calculated similarly to Peduto et al. (2017) and Peduto et al. (2019), by (1) creating greenfield ground surface settlement profiles from the grid results along the x- and y-directions, (2) deriving the settlement profiles inside buildings by intersecting building shapes crossing the profile, (3) calculating the damage parameters on each building-specific settlement profile and (4) extracting the maximum value of each damage parameter for comparison with damage criteria.

The following commonly used damage criteria were investigated for comparison: Rankin's (1988) method, the State-of-strain Method (SOSM) (Son and Cording, 2005) and the Limiting Tensile Strain Method (LTSM) (Burland and Wroth, 1974). The settlements were computed with a 2D rate-dependent hydro-mechanical (HM) model and extrapolated over a large area using hydro-stratigraphic features within a metamodel. A metamodel is a computationally effective surrogate model to approximate a detailed numerical model (Blanning, 1975). Such a model generally does not replicate the physical processes of the underlying time-dependent numerical model, but is enabled to learn the relationship between the model inputs and outcomes, see e.g. Fienen et al. (2018), Furtney et al. (2022), Kang et al. (2017), Ninić and Meschke (2015), Obel et al. (2020) and Wang et al. (2016).

In the 2D HM model, tunnel leakage is emulated by simulating instant uniform drawdown in the confined aquifer below the soft clay layer, followed by a fully coupled consolidation analysis with an advanced rate-dependent model. As the purpose is to assess potential damage at a district scale, the influence of the foundations on the predicted settlements was not considered in this phase. Namely, this would require much more detailed 3D numerical studies coupling groundwater flow, soil deformations and the foundations. Yet, conservative results are still mostly assured as foundations are much stiffer than surrounding clay, and thus would reduce the predicted total and differential settlements.

Fig. 1 shows the general strategy adopted. In step 1, settlement data from a considered drawdown scenario were generated by the 2D hydro-mechanical model and used as training and validation data for a metamodel. The settlement data were assembled in grids of x (east–west) and y (north–south) coordinates with a spacing of 5 m in both directions. This step also works for other settlement predictions or measurements, as long as they are on a grid of equal spacing.

In step 2, polygon and building type data were collected from the database of the actual construction project. The generated and collected data were then used as input in the building damage model.

In step 3, the settlement data were reassembled into profiles of constant x (aligned in north–south direction) or y (aligned in east–west direction) coordinates to calculate 2D building damage parameters, using the chosen empirical and semi-empirical methods. Since the profiles only are calculated in two directions, such an approach does not always consider the worst settlement profile, which may be in another direction. For building polygons to interact with the settlement data, intersection points were created, where the building polygons and the profiles intersect, to be used as endpoints for the creation of building-specific profiles. Settlement data within two intersection points were saved inside the building-specific profiles. The benefit of also including points inside the building, rather than just external walls, is that the approximate settlement effects on inner walls can be included.

In step 4, the chosen building damage parameters are calculated within each building-specific profile. Since the buildings intersect with several settlement profiles (albeit in two directions), the maximum value is saved for the following steps. In step 5, calculated damage parameters are then compared with respective damage criteria, with damage classes assigned for each building. In step 6, a comparison is made between the different damage criteria in terms of how many buildings are in each damage class per damage criteria.

In step 7, a new iteration with a different drawdown and consolidation time scenario is used as input to the hydro-mechanical model at which step one starts again. This step was important for understanding how quickly each drawdown scenario is felt, to set up an infiltration programme to mitigate the settlements. Finally, in step 8, the comparison of damage criteria for different pore pressure drawdown and consolidation time scenarios enables useful recommendations for a first-stage damage assessment at a large area, based on comparisons of the output from the different damage criteria, correlations between damage parameters used in each criterion and their complexity. All steps are processed with code written in MATLAB.

For correlation, the Spearman rank correlation coefficient was used (see e.g. Agresti and Franklin (2007)). The Spearman rank correlation coefficient is a non-parametric measure of the correlation between the rankings of two variables having a monotonic (only positive or negative) relationship. Since it is a measure of correlation between rankings rather than observed values of the variables, it is not restricted to linear relationships in contrast to the Pearson correlation coefficient. The Spearman rank correlation coefficient was chosen here since non-linear relationships could not be excluded. The Spearman rank correlation coefficient ($-1 \geq r_s \leq 1$) is:

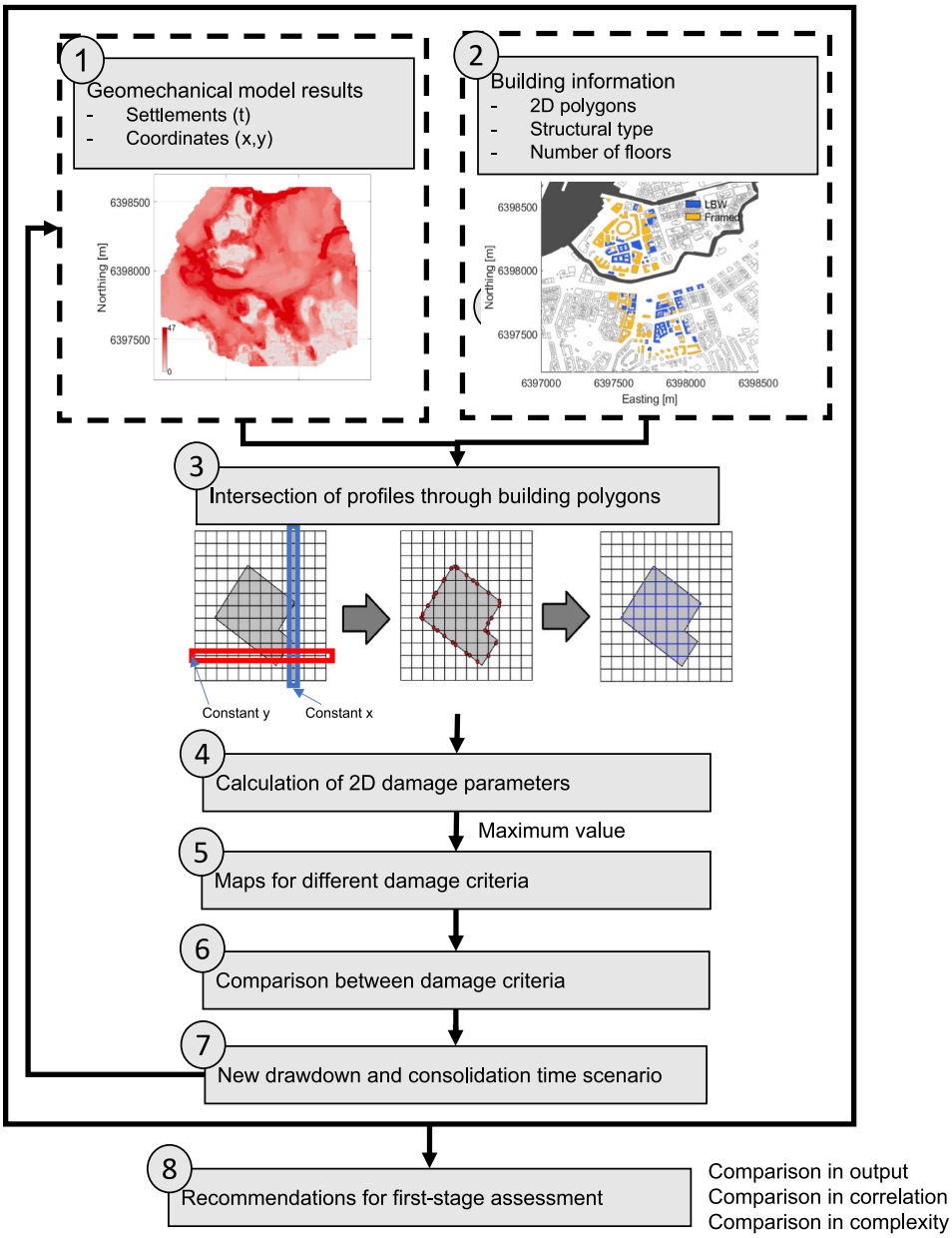

Fig. 1. General strategy of the building damage model.

$$r_s = \frac{COV(R(X), R(Y))}{\sigma_{R(X)}\sigma_{(R(Y)}}$$

where *COV(R(X),R(Y))* is the covariance of the ranking integers *R* of variables *X* and *Y* and σ is the standard deviation of ranking integers *R*.

2.2. Underlying models

The proposed building damage model is a stand-alone model which can use any type of 3D settlement data aligned as a grid. However, to demonstrate its practicality, several recently developed models were used to create the settlement data. A flowchart of these underlying

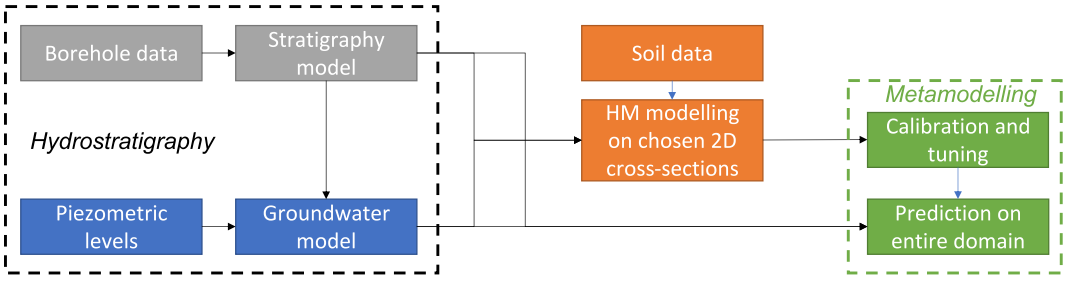

Fig. 2. Flowchart of underlying models to produce settlement data.

models is shown in Fig. 2.

Firstly, a geostatistical stratigraphy model using existing borehole data to retrieve the soil/rock layering was used to determine the stratification in the model with a resolution of 5x5m (Sundell et al., 2016). Secondly, a MODFLOW groundwater model was set up using the stratigraphy model and calibrated on observed groundwater levels to retrieve piezometric maps of the upper (unconfined) and lower (confined) aquifer at a resolution of 5x5 m.

Thirdly, a hydro-mechanically (HM) coupled finite element model (adopted from Wikby et al. (2023)) was set up in PLAXIS 2D version 21. An in-house implementation of the rate-dependent model Creep-SCLAY1S (Gras et al., 2017; Gras et al., 2018; Sivasithamparam et al., 2015) was used to model the response of the clay layer. Creep-SCLAY1S has been shown to replicate the soft clay response, i.e. creep, anisotropy and debonding, through system-level benchmarking (validation in terms of pore pressures, lateral and vertical settlements with depth) in several projects in Sweden (e.g. Bozkurt et al. (2023), Tornborg et al. (2023), Tornborg et al. (2021)) and elsewhere (e.g. Amavasai et al. (2017) and Amavasai et al. (2018)), involving both excavations and embankments. Using soil data from oedometer and triaxial tests, the model parameters were calibrated. Additionally, a bellow hose, which provided depth-integrated absolute settlement data, was used for model calibration, thus ensuring that the ongoing background creep deformation is accounted for using the adopted model and state parameters. In total, six sublayers for the clay were assumed based on the soil property profiles.

Fourthly, the results needed to be extrapolated over a large area. Instead of using a point-wise one-dimensional settlement model, a metamodel was set up to scale up the model results from the 2D HM model over a large area. The results from three cross-sections (all between 600 and 1000 m in length) simulated in PLAXIS using the HM model were used to retrieve the displacements and their relation to the hydro-stratigraphic data, corresponding to a given drawdown scenario and consolidation time. Two cross-sections were used to train the metamodel, while a third one was used for validation. A statistical learning framework was used to train the metamodel on the results of the simulated cross sections, using features such as hydro-stratigraphy available for the entire domain. This way we get subsidence predictions on the entire model domain for the building damage model that is the focus of this paper.

2.3. Creation of building-specific profiles

Fig. 3 illustrates how settlement profiles in one example building were calculated. Grid-based settlements and building polygons in a shapefile (Fig. 3(a)) are first imported and divided into 2D settlement profiles with constant x- (going north to south) and y- (going east to west) coordinates. Intersection points are then calculated along the profile (two along each building segment). These two points then represent the first and last point on a building-specific profile. Settlement points within the polygon are saved into 2D settlement profiles (Fig. 3(b)). Thereafter, settlements on the intersection points were linearly interpolated from the neighbouring points. The resulting profiles are shown in Fig. 3(c) for each building segment. This process is then iterated for all "global" settlement profiles and building polygons.

2.4. Calculation of damage parameters

Several parameters to assess the settlement-induced damage have been proposed. Burland and Wroth (1974) considered relevant parameters for 2D damage criteria, namely total settlements (S), rotation (θ), rigid body tilt (ω), angular distortion (β), angular strain (α), relative deflection (Δ), and deflection ratio (Δ/l_Δ). l_Δ in this case represent the total horizontal length at which one deflection mode is dominant, which could either be hogging (downward concavity) or sagging (upward concavity). θ is defined as the inclination between two neighbouring settlement points. ω is the inclination between each wall edge (in this case the two intersection points of a profile). The angular distortion is calculated as $\beta = \theta - \omega$ for each point. The latter three parameters are considered positive in a counterclockwise direction. Angular strain is calculated as the difference between two neighbouring rotation values ($\alpha_i = \theta_{i,i+1} - \theta_{i-1,i}$). It represents the current deflection mode according to Burland and Wroth (1974), as positive values represent sagging and negative values represent hogging. Theoretically, locations where $\alpha = 0$ represents inflection points. Fig. 4(a-d) shows examples of how the parameters are calculated, where points 1 and 2 are the ends of a deflecting section, and point A is the point closest to point 2.

Fig. 5 shows an example of how each of these parameters is calculated, and based on the series of angular strains, how inflection point locations and inflection lengths l_Δ are derived for a typical settlement

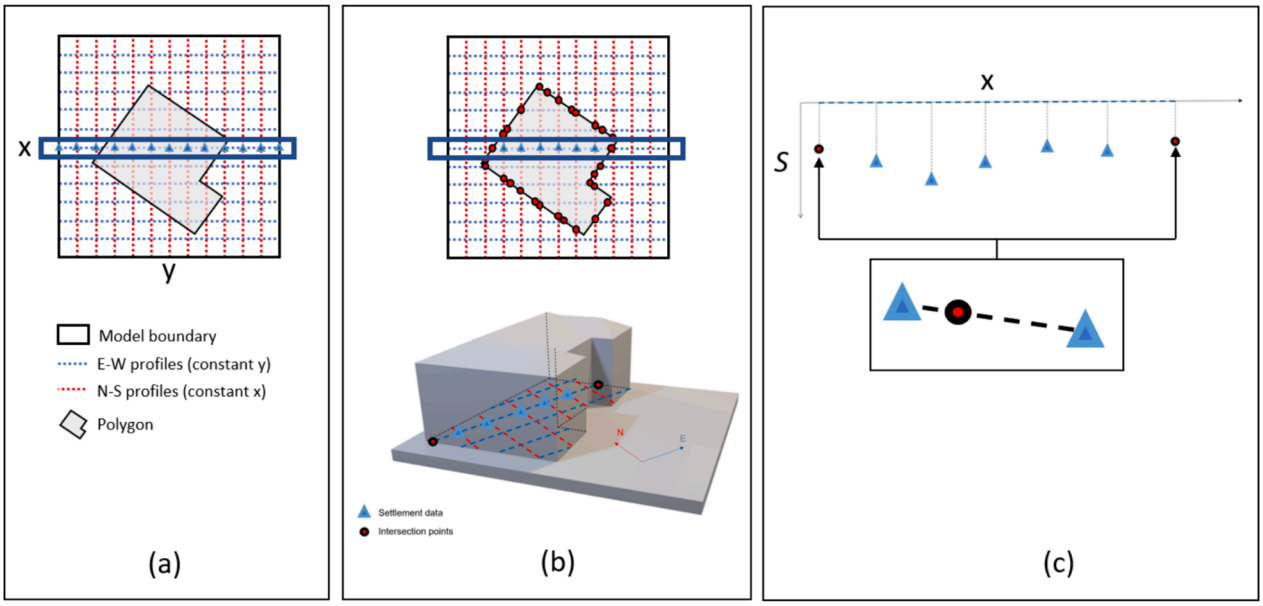

Fig. 3. Conceptual map of how a building-specific settlement profile was derived. (a) Selection of settlement profile from the grid. (b) Creation of intersection points and building-specific settlement profiles. Points inside the building polygon are saved. (c) The final settlement profile, as shown from above in (b). Settlements are interpolated on the intersection points between two nearby data points on the "global settlement profile".

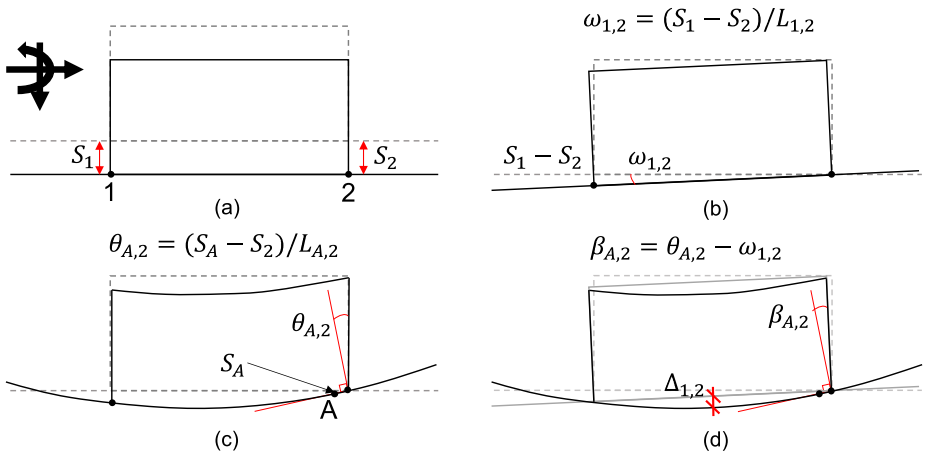

Fig. 4. Examples of geometrical assumptions underlying damage parameters and how they are calculated. Rotation in a counterclockwise direction is considered positive. (a) Case of uniform settlements. (b) Case of rigid body tilt. (c) Case of rotation. (d) Case of both rotation and tilt (angular distortion and relative deflection).

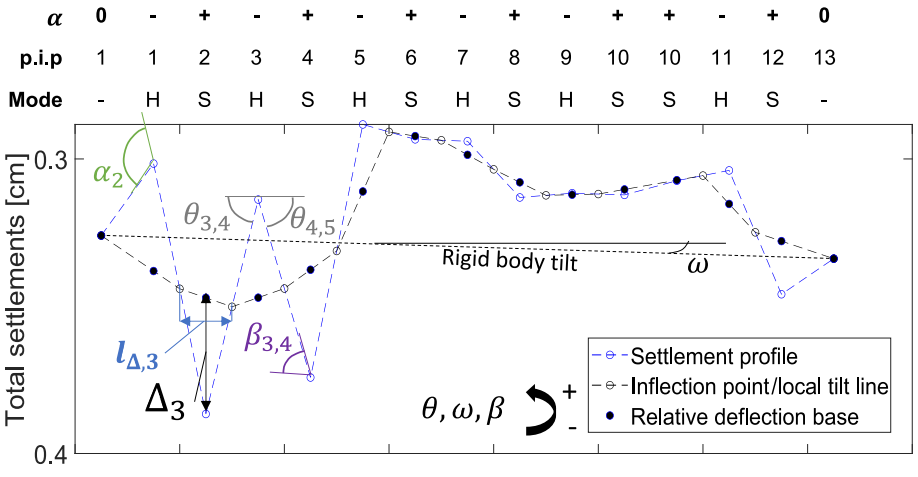

Combinations of angular strains	$l_\Delta/\delta l$	Mode
$\alpha^+ + n\alpha^- + \alpha^+$	n	Hogging
$\alpha^0 + n\alpha^- + \alpha^+$	$n + 0.5$	
$\alpha^0 + n\alpha^- + \alpha^0$	$n + 1$	
$\alpha^0 + n\alpha^+ + \alpha^0$	$n + 1$	Sagging
$\alpha^0 + n\alpha^+ + \alpha^-$	$n + 0.5$	
$\alpha^- + n\alpha^+ + \alpha^-$	n	

α = angular strain
p.i.p = Passed inflection points
H = Hogging
S = Sagging

δl-length between two calculated points

$\alpha^+: \alpha > 0$
$\alpha^0: \alpha = 0$
$\alpha^-: \alpha < 0$

Fig. 5. Example profile of how inflection lengths, relative deflection, deflection lengths and deflection ratios were derived. Angular strains, calculated at each profile coordinate, determine the mode of deflection at that point. Intersection points (the first and last point on the settlement profile) also count as inflection points.

profile of a building. First, a vector is calculated that represents the number of inflection points along the settlement profile (including intersection points). This is based on how often α switches from positive to negative, and vice versa. Where α switches sign from one point to the next, the inflection point is assumed to lie between the two points. An example is shown in Fig. 5, where the inflection length was calculated where n inflection points were passed. Based on where the inflection point crossed the settlement profile, the total settlements at each inflection point were calculated. A local tilt line was created between two inflection points and on that tilt line, the settlements were interpolated. Finally, the relative deflections were calculated between the main settlement profile and the local tilt line for each settlement point and the deflection ratio.

Depending on how many passed inflection points each coordinate has on the building-specific settlement profile, that specific inflection length is saved. In the example in Fig. 5, 12 inflection lengths are calculated. These are grouped with each relative deflection to calculate the deflection ratio.

This process is repeated for all buildings in the study domain. For each building, the maximum total settlement, rotation, angular

distortion and deflection ratio are retained representing the worst-case scenario. Since the inflection length was grouped with the deflection ratio, it is retained for later calculation of Limiting Tensile Strain (LTSM).

2.5. Selecting damage criteria

Table 1 shows the damage criteria used for the building damage models. One damage criterion using empirical methods was chosen, as well as two semi-empirical methods.

The empirical damage criterion is based on Rankin (1988) considering total settlements and rotation. The most conservative value of the two parameters in this simple criterion is widely used in first-stage assessments of deep excavation problems (Mair et al., 1996; Son and Cording, 2005).

The semi-empirical criteria are the 2D State-of-Strain Method (SOSM) (Boscardin and Cording, 1989; Son and Cording, 2005) and the Limiting Tensile Strain Method (LTSM) (Burland and Wroth, 1974) to highlight the adaptability of the proposed method. These have been widely used in second-stage assessments in practice, e.g. the Jubilee line extension project in London, United Kingdom (Burland et al., 2004) and the North-South Metro project in Amsterdam, Netherlands (Korff, 2013). In general, these criteria assume centrally loaded façades with rectangular shapes and homogeneous linear elastic material in plane strain conditions. SOSM further assumes a fixed stiffness ratio, neutral plane and length-to-height ratio for the building to accommodate experience-based conservative conditions and uses the angular distortion parameter instead of deflection ratio. Burland et al. (2004) argued that the angular distortion parameter is more ambiguous, as it depends strongly on the load distribution compared with the deflection ratio parameter. Experience has, however, shown that diagonal cracking due to shearing is generally more critical, best represented with the angular distortion parameter, thus favouring the simpler SOSM (Son and Cording, 2005). Both arguments are valid, hence, both parameters were studied.

While the semi-empirical criteria are efficient and easy to adopt in the proposed methodology, they come with limitations compared to numerical methods as discussed in Dalgic et al. (2018), mainly in geometry, 3D effects, loading conditions, pre-existing conditions, the effect of non-linearity and heterogeneity of the façade material stiffness and strength, and the influence of foundation stiffness. However, in the case of buildings with large surface areas assessed with the proposed methodology, several green-field settlement profiles are assessed simultaneously which could compensate for the limitations. In cases where a building strongly deviates from the assumptions of the semi-empirical methods as well as where soil-structure interaction is important, numerical methods are preferable.

The applied classification system contains five classes according to Burland et al. (1977): negligible, very slight, slight, moderate and severe. As a reference, these classes are equivalent to aesthetic, functional and structural damage. The compatibility between the well-established parameter boundaries, observed damage and crack width has been confirmed by e.g. Dalgic et al. (2018).

Some modifications had to be made for the purpose of the study. For LTSM, the maximum total tensile strain $\varepsilon_{t,max}$ is calculated as the maximum of the tensile shear strains and bending strains as proposed by Burland and Wroth (1974). The relative building stiffness (E/G) was chosen as 2.6 for the load-bearing walls and 12.5 for the framed structures according to Burland and Wroth (1974). Finally, the maximum of each parameter is calculated for each building and the damage class is determined based on the classification in Table 1.

Table 1
Damage classification table with the different criteria.

Method				SOSM	LTSM
Main reference		Rankin (1988)		Son and Cording (2005)	Burland and Wroth (1974)
Category		S [mm]	θ [–]	β[$\times 10^{-3}$]	$\varepsilon_{t,max}$[%]
Aesthetic	N.	0–10	0–1/500	0–1	0–0.05
	V.		–	0–1	0.05–0.075
	Sl.				
	Sl.	10–50	1/500–1/200	1.5–3.33	0.075–0.15
Functional	M.	50–75	1/200–1/50	3.33–6.67	0.15–0.3
Structural	S.	>75	>1/50	>6.67	>0.3

3. Case study

3.1. Problem description

The method was applied to buildings in three districts of Central Gothenburg, Sweden (Haga, Vasastaden and Inom Vallgraven), where a new underground railway tunnel and station are being built (Fig. 6). The construction of an unlined pre-grouted tunnel in hard crystalline rock will cause some leakage of groundwater into the subsurface construction, with the potential to cause a gradual time-dependent pore pressure reduction in the overburden soft soils. This pore pressure reduction may in turn result in time-dependent ground deformations, due to consolidation and creep. As the clay layer is underlain by a permeable layer of coarse-grained materials, and permeable fracture sets, the impact of leakage may manifest up to several hundreds of meters away from the actual construction unless timely mitigation measures (additional sealing and infiltration) are implemented (Trafikverket, 2014). The building damage model is constructed for an area of about 1.5x1.5 km^2, expected to be influenced by leakage. Four different hypothetical drawdown scenarios at different consolidation times are considered, enabling assessment of the potential short-term damage during the construction and the long-term damage, when the facilities are in use.

3.2. Geology

The area consists of deposits of soft sensitive marine clay formed during and after the last Ice Age (glacial and post-glacial clay). The clay was deposited on top of glacial till, occasional glaciofluvial coarse-

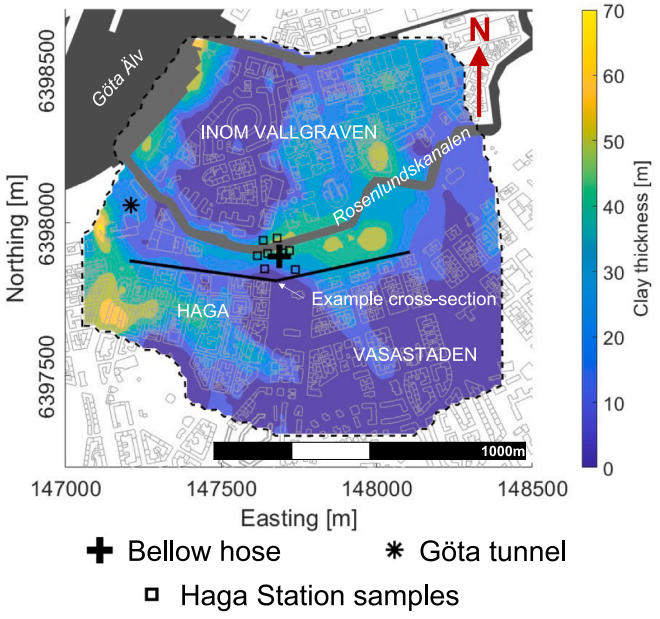

Fig. 6. Case study data locations in the model domain, including the clay thickness.

grained sediments (sand-gravel) and hard crystalline rock, which at the top may be heavily weathered and fractured. Due to a strongly undulating bedrock surface, clay deposits reach depths of up to 70 m in some locations, whilst at other locations the bedrock is exposed as seen in Fig. 6. On top of the clay deposits, there are beach deposits and fill materials. The top five meters of clay (fill) have been heavily altered, due to the construction of buildings and utilities, as well as land reclamation using dredged materials from the nearby canal (Trafikverket, 2014). Thus, different loading situations, both natural and anthropogenic, have led to ongoing background creep settlements of 2–5 mm/year (TreMaps, 2022).

3.3. Hydro-mechanical modelling data

Oedometer and triaxial tests were performed to derive relevant model parameters for the soft clay. Fig. 7(a) displays the key index properties (density, natural water content, sensitivity, vertical hydraulic conductivity and over-consolidation ratio) derived as a function of depth. These properties are compared with the properties from the well-characterised Göta tunnel project (Tornborg et al., 2021), shown in Fig. 6. Fig. 7(a) shows that the properties of both sites are similar. The deviations in the water content at 20–30 m depth are most likely due to the proximity to the frictional layer, attributed to the relatively shallow clay thickness at the Göta tunnel site. Given most model parameters are intrinsic properties, the values of Tornborg et al. (2021) were adopted for the simulations, with site-specific values of OCR (vertical over-consolidation ratio). These site-specific values were calibrated through the bellow hose (Fig. 7(b)) at great depths, as the oedometer results indicated poor sample quality at great depths (displayed as red squares in Fig. 7(a)). As shown in Fig. 7(b), with these calibrated parameters it is possible to reproduce the background creep settlements as a function of depth between 2011–2018.

The hydro-stratigraphic data, derived based on borehole logs and groundwater levels, are further displayed for one of the cross-sections in Fig. 7(c) together with the FE mesh. Representative scenarios of a pore-water pressure drop in the lower aquifer (due to leakage to the tunnel) were chosen, and 2D sections of the domain were simulated with the 2D HM model. Mesh independence was ensured by adjusting the average element size.

3.4. Considered scenarios and input from hydro-mechanical model

The hydro-mechanical model was applied to a case where the piezometric head was lowered in the confined aquifer (till) to emulate leakage into a tunnel. This results in drainage starting in the lower boundary of the clay layer and continuing upwards (underdrainage), see Fig. 8, resulting in consolidation and creep from the bottom up. Thus, it was important to calibrate the model to reproduce the background creep

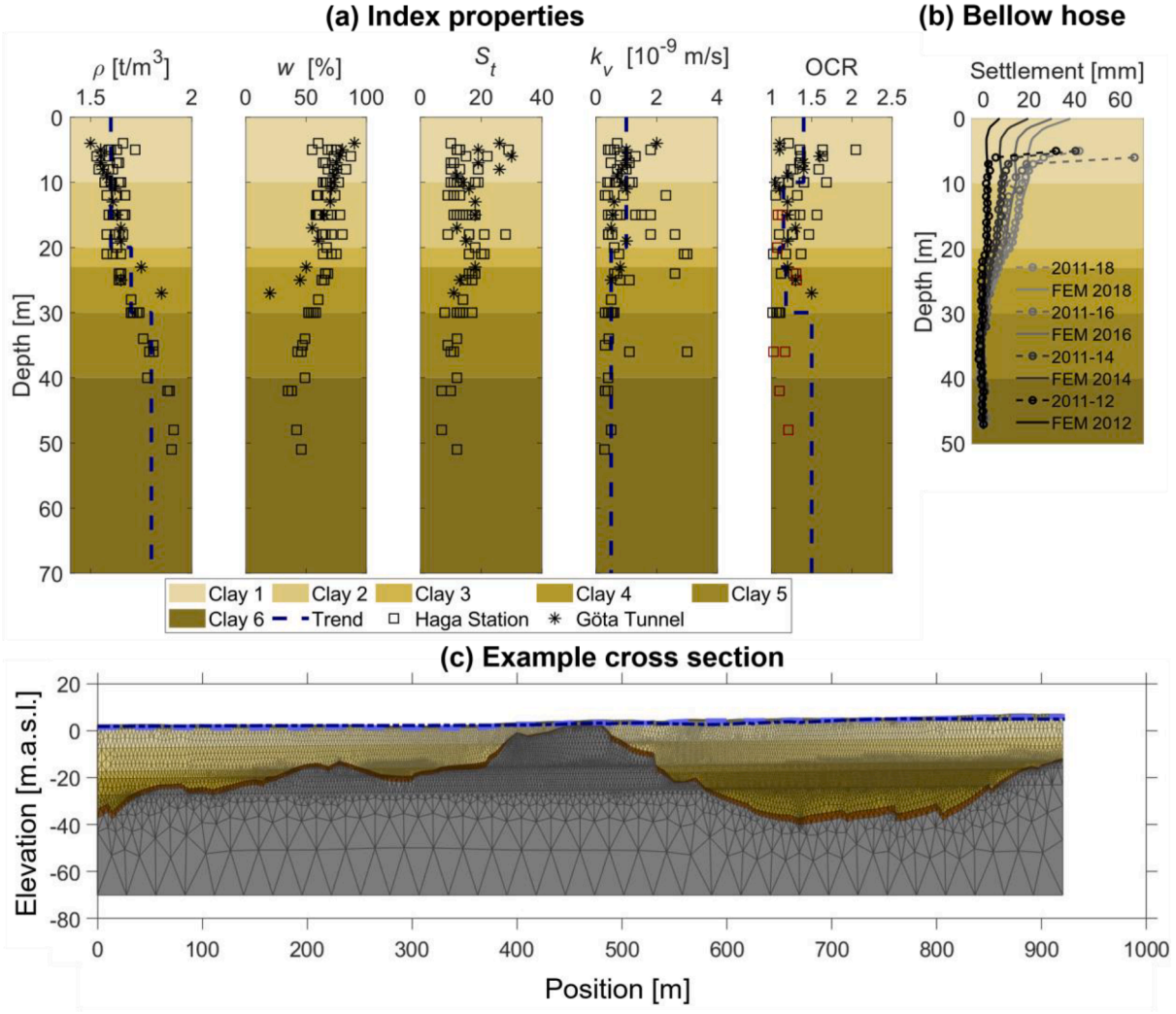

Fig. 7. Hydro-mechanical modelling data. Locations can be found in Fig. 6. Soil properties displayed are density (ρ), natural water content (w), sensitivity (S_t), vertical hydraulic conductivity (k_v) and over-consolidation ratio (OCR).

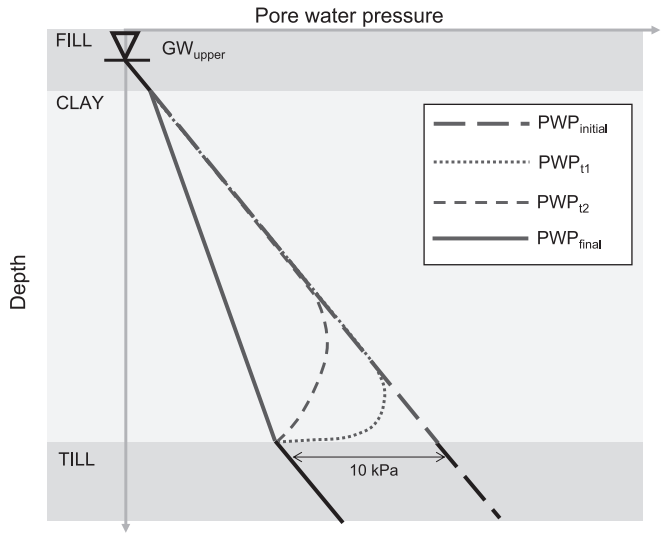

Fig. 8. Excess pore pressure dissipation process of a typical underdrainage problem in clays bounded by an upper and a lower aquifer (modified from Wikby et al. (2023)).

settlements. As a result, most soil displacements should therefore occur in the soil closest to the confined aquifer similarly to e.g. Tianjin, China (Zeng et al., 2021, 2022b; Zeng et al., 2019; Zheng et al., 2019). Fig. 8 further shows the pore pressure gradients of the initial state, states of consolidation times t1 and t2, as well as the final consolidation state. To consider the worst-case scenario, the drawdown was uniformly distributed in space. In this paper, the scenarios considered 10 kPa and 40 kPa pore water pressure drop at the bottom of the clay layer, representing a case with virtually no leakage and a case that is considered the worst-case scenario based on local experience. The computed settlements after 1 year and 30 years of consolidation are subsequently used as input for the building damage model.

3.5. Studied buildings

In the three districts of Central Gothenburg considered, 215 buildings with detailed inventories e.g. structural type, foundation type, number of floors, age, foundation level and observed damage were identified in the model area (Fig. 9(a)). Since the description of each typology in the inventory was initially uncategorized, the structural type was first systematically classified into two categories: Load-bearing walls (LBW) and framed structures. This categorization is based on the assumed relative flexibility of the structure in shear, with framed structures considered as much more flexible in shear (see e.g. Burland and Wroth (1974)). The categorized LBW buildings included (1) Wood frames with masonry façade, and (2) LBW of masonry or reinforced concrete (RC). Categorized framed structures included (1) steel-framed or RC structures, even including masonry walls or similar, and (2) timber structures. This categorization was used to determine the relative bending-to-shearing stiffness (used in LTSM) of each building, which is one of the variables needed to calculate the maximum tensile strain.

Based on this categorization, there are 112 buildings with load-bearing walls (LBW), whilst 103 buildings were considered as framed structures in their response, see Fig. 9(a). LTSM requires the input of height. Thus, the total number of floors was used to estimate the building height, with each floor assumed to be 3 m, see Fig. 9(b). Building weight, existing openings and possible asymmetries in the building were not considered.

Fig. 9(c) and 9(d) show the foundation types and classified vulnerability. The foundations were classified into three categories, shown for comparison with observed damage. For 208 buildings in the study area, consultants conducted building damage protocols prior to tunnel construction as a basis for a three-class vulnerability classification (see Table 2). For this classification to be comparable to the building damage model proposed here, the vulnerability was reclassified into “validation classes” to be comparable to one or several of the damage classes proposed by Burland et al. (1977) (see Table 2). For instance, high vulnerability according to the consultant system is potentially equivalent to slight damage as it is highly unlikely that any of the previously damaged buildings have functional or structural damage.

The validation of computed predictions vs. observed damage was later assessed with contingency tables (Gokhale and Kullback, 1978), to determine the overlap of each class and scenario. SOSM and LTSM were chosen because they are believed to be the most accurate methods correlated to damage. In each table cell, a percentage of a particular combination between two discrete random variables (computed and observed damage classes in our case) is calculated. Thereafter, the chi-squared value and subsequent p-value are calculated for each table. For chi-squared computation, the predicted damage classes slight to severe are combined due to insufficient information on the observed damage. A high p-value means a high significance of the model validation class. Vulnerability classifications were not found for seven buildings and those were thus excluded from the contingency analysis.

4. Results of case study

4.1. Settlement results

Fig. 10 displays the computed settlements for the imaginary pressure drops of 10 kPa and 40 kPa, considering consolidation times of 1 year and 30 years, respectively, on the entire model domain. Fig. 10(a) displays the least settlements, while Fig. 10(d) shows the most, reflecting the magnitude and duration of the drawdown on the induced settlements. Fig. 10(d) (40kPa30y) also shows a rather drastic change in settlement magnitude along the soil–bedrock interface, i.e. 50–150 m from the outcrops, where the largest settlements can be found. Similar observations were made from the scenarios 10kPa1y and 40kPa1y.

4.2. Building damage results

Fig. 11 shows maps for different damage parameter values (left), the damage maps based on each criterion (middle), as well as the settlement results (right) for the scenario with 10 kPa pressure drop with 30 years of consolidation. In general, the buildings in the northeast and southwest show relatively low magnitudes and damage for all other damage parameters and criteria than for total settlements and Rankin (S), respectively. These are areas located 50–150 m from the rock outcrops, where the largest settlements can be found due to deep clay layers. Fig. 11 also demonstrates that SOSM and LTSM are rather comparable.

Fig. 12 compares the results based on different damage criteria using a bar plot (left axis) and a supporting cumulative diagram (right axis). Regarding the cumulative diagram, a subtler increase is tied to increased damage severity based on the damage criterion. In general, SOSM and Rankin (S) yielded the most severe results, where the difference in trend is scenario-dependent, e.g. SOSM for 40kPa1y (Fig. 12(c)) is more severe and Rankin (S) for 10kPa30y (Fig. 12(b)). In contrast, Rankin (θ) appears to be the least severe for all scenarios. Furthermore, Fig. 12 displays a general increase in severity with increased drawdown magnitude and duration for all criteria, which is in line with expectations.

Fig. 12(a) shows that most criteria yielded negligible damage, and thus such a limited pressure drop during the construction time is expected to cause limited damage to only a few buildings. For long-term and larger pressure drops most criteria predict severe damage to most buildings in the area (Fig. 12d). For the remaining scenarios shown in Fig. 12(b-c), the severity is rather similar, except for Rankin (S). Rankin (S) is more severe in the case of 10 kPa 30 years, when ca 70 % of cases fall into the Severe category. In Fig. 12(b), Rankin (S) acts as an upper boundary. Similarly, to Fig. 11, a lower damage can be seen for Rankin

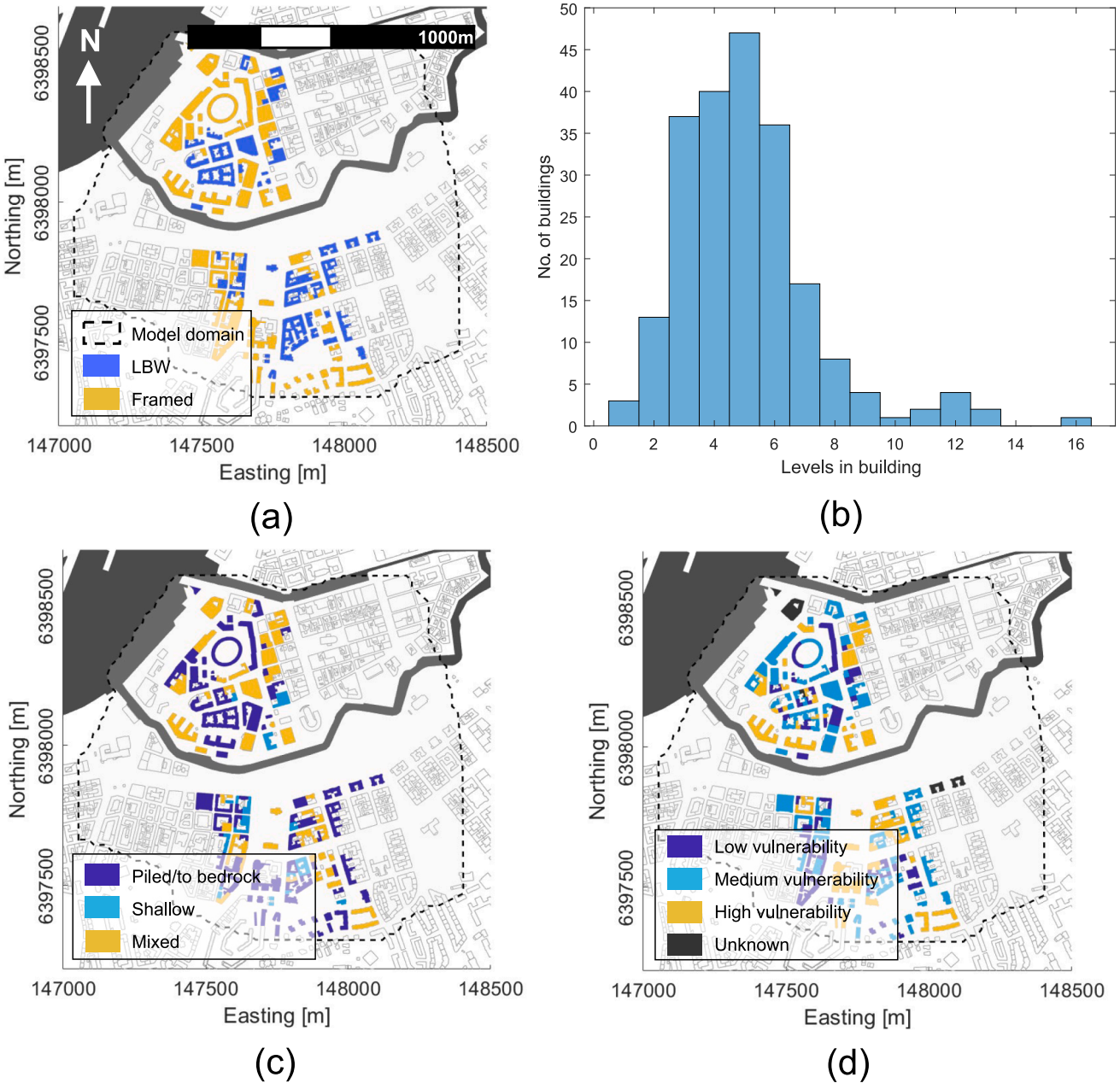

Fig. 9. (a) Structural type map with model domain in surroundings. LBW = Load-bearing walls, Framed = Framed structures. (b) Number of levels in each building. (c) Foundation-type map. (d) Vulnerability map.

Table 2
Damage classification and assumptions of equivalent damage.

Damage class*	Crack width*	Vulnerability class**	Validation class***
Negligible	<0.1 mm	Low	A
Very slight	0.1–1 mm	Medium	B
Slight	1–5 mm	High	C
Moderate	5–15 mm	High	C
Severe	>15 mm	High	C

*Burland et al. (1977) system, **Consultant's system, ***Used in validation

(θ) than for SOSM.

4.3. Comparison of damage parameters and criteria

Table 3 displays the correlation between the maximum values for damage parameters of all buildings for the 40 kPa 1-year scenario using the Spearman rank correlation coefficient (r_s) which considers the statistical dependence between the rankings of two variables. Table 3 shows that the rotation and angular distortion are correlated the most, followed by angular distortion-limiting tensile strain or rotation-limiting tensile strain, depending on the magnitude and time of consolidation. Moreover, the total settlement parameter constitutes by far the lowest correlation with all other damage parameters, especially limiting tensile strain. These correlations differ most likely due to the difference in the complexity of the methods.

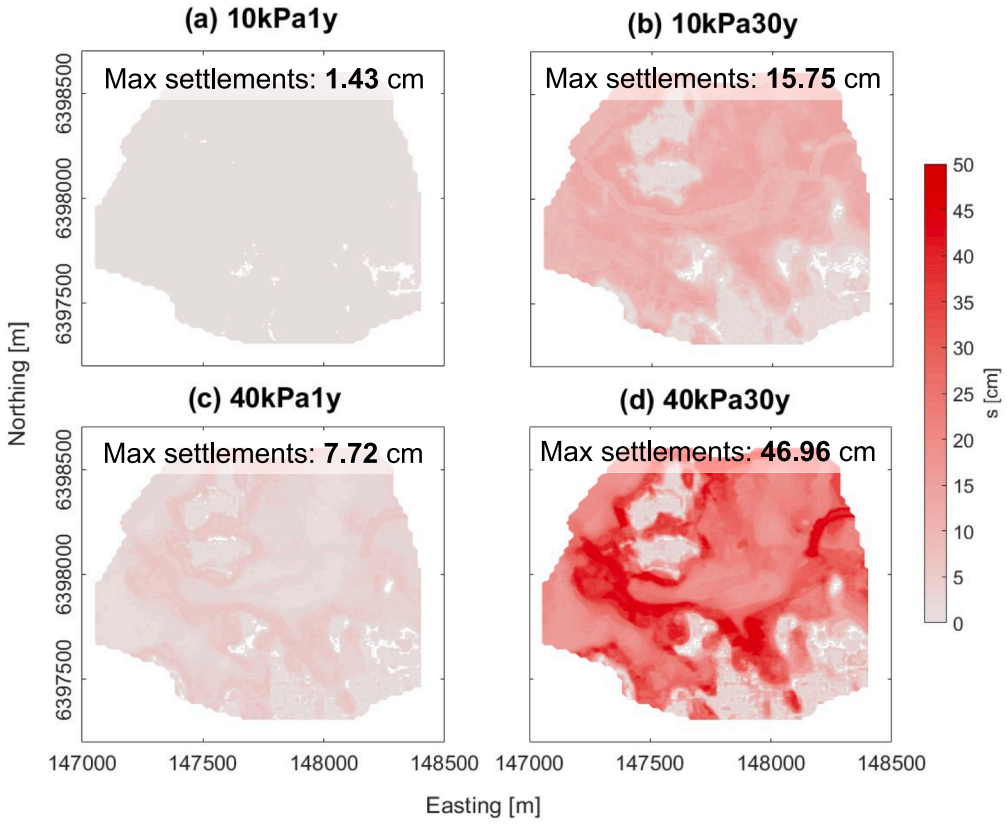

Fig. 10. Settlement results for the different scenarios (in cm). Red scale ranging from 0 to 10 cm.

Despite rotation and angular distortion being very similar (r_s = 0.98), the Rankin criterion for rotation and SOSM criterion yield different results (Figs. 11 and 12), which means that the results may be sensitive not to the chosen parameter, but in contrast sensitive to the limits for the damage category.

Fig. 13 illustrates two examples of damage parameter comparison. It shows a positive trend in both examples, supporting the assumption of a monotonic relationship. Based on the results from Table 3, angular distortion vs. total settlements (Fig. 13(a)) and maximum tensile strain vs. rotation (Fig. 13(b)) are shown here. Fig. 13(a) displays a wide scatter with local clusters formed by each scenario. The reason for the wide scatter in the scenario clusters could not be identified, even after attempts at relating the scatter to the length-to-height ratio of a building, or to the area of the building polygon (larger polygons imply more settlement points, and thus a shift in maximum values in relation to its total distribution). On the other hand, the low correlation could be an indication that a certain percentage of the total settlements are uniform, i.e. there is no rotation. A higher correlation was seen for the 10 kPa 1-year scenario where only small settlements (<1cm) were computed. Fig. 13(b) shows less clustering. The deviation from the mean trend could be tied to differences in structural type and geometry, but also differences in deflection shapes and their relation to the rigid body tilt.

4.4. Validation of predicted damage

Tables 4-7 show the contingency table analysis for all scenarios. Each cell shows the percentage of buildings in one combination. 10kPa30y, 40kPa1y and 40kPa30y show mostly overpredictions while 10kPa1y show mostly underpredictions. Moreover, the evaluated p-values are not significant (i.e. < 0.05) for any scenario. An indication of other causes of damage than pure creep settlements is likely the reason. For instance, previous loading, groundwater lowering due to construction of infrastructure or blasting of rock could be the reason for damage. Possibly, these buildings have deteriorated over time.

4.5. Resolution of hydro-mechanical model results

Fig. 14(a-b) show the settlement and rotation uncertainty range when different resolutions are used for settlement profiles A-A (a) and B-B (b). The uncertainties for each resolution were derived after recording each point on the settlement profile and plotting the 5th, 25th, 50th, 75th and 95th percentile. Their locations are found in Fig. 14(c). The upper parts of Fig. 14(a-b) show how the settlement profiles change with decreased resolution. Even though the chosen profiles are considerably longer than the footprint of the building, similar results can be seen for several profiles. Thus, the results suggest that somewhere between 20–30 points within a profile will capture the total settlement uncertainty of higher resolution. The bottom parts of the figures show that the total settlement uncertainty can be captured with just 26 points. On the other hand, the uncertainty and maximum values in rotation increase with higher resolution. It is, however, likely that due to soil-structure interaction effects, the high rotation values are unrealistic (in this case the maximum rotation would be 2.5 % for 256 points).

Fig. 15 shows how the predicted results are changing with decreased resolution, from 5x5m to 10x10m for each damage category. In general, the results do not change much, meaning that the predicted damage is not that sensitive to spatial resolution, although a slight decrease in the severity of the damage can be seen for most criteria. However, judging from the discussion above, an increase in resolution (and thus sample size in a settlement profile) should increase the severity of the results.

5. Discussion

This study presents an approach for constructing a building damage model based on settlement profiles extracted from grid-type settlement predictions for a large area. Some of the largest uncertainties in the

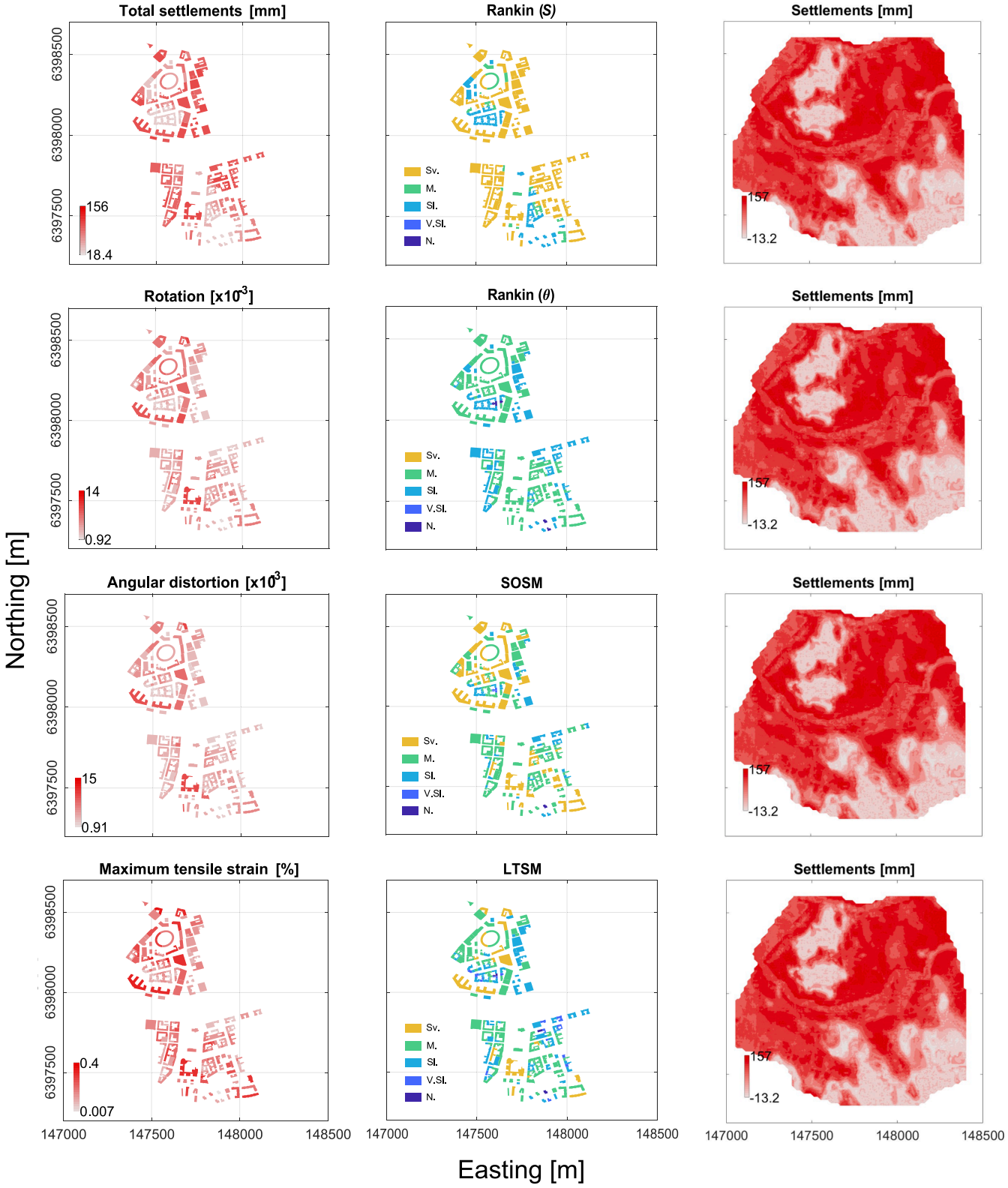

Fig. 11. Results from 10 kPa 30 years of consolidation scenario. On the left, are results from the predicted maximum value of each damage parameter. In the middle, are results from the predicted damage category based on limits proposed by authors. On the right, settlement results from the metamodel are displayed for comparison. N. – Negligible, V.Sl. – Very slight, Sl. – Slight, M. – Moderate, Sv. – Severe.

proposed method include the assumptions of using the maximum value of each parameter, the deflection shape, the grid resolution, the influence of building and foundation stiffness on settlement profile, the neglection of previous damage as well as neglection of horizontal strains. The uncertainties due to the latter three issues are discussed in the following.

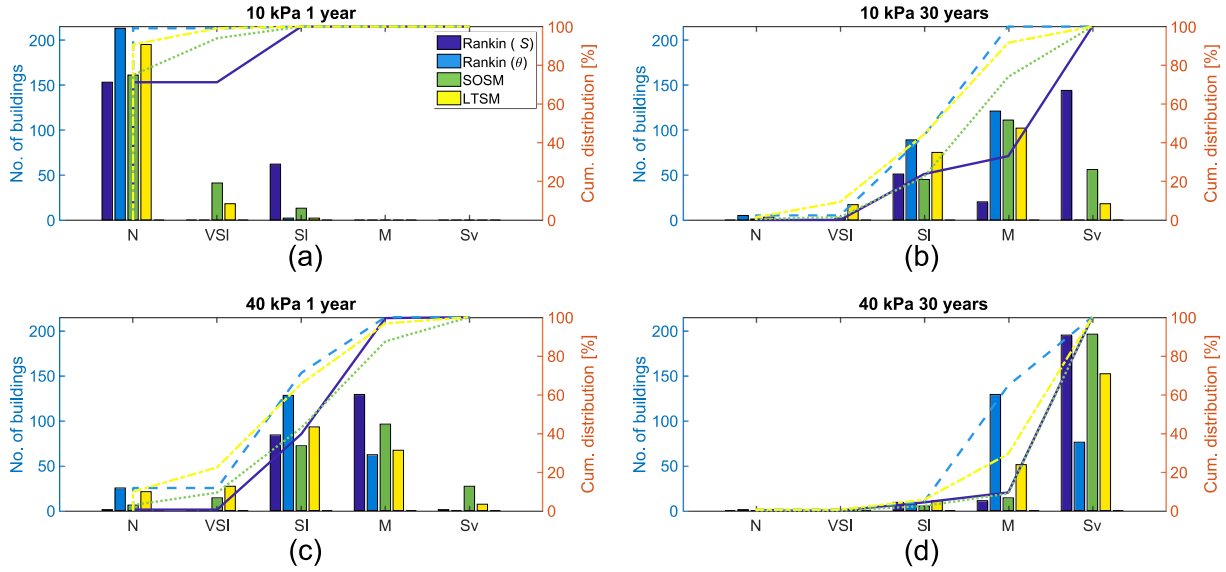

Fig. 12. Comparison of damage criteria on evaluated damage classes.

Table 3
Spearman rank correlation coefficients (r_s) for different damage parameters for 40 kPa 30 years.

r_s	Total Settlements	Rotation	Ang. Distortion	Lim. Tens. Strain
Total settlements	1	0.12	0.04	0.01
Rotation	0.12	1	0.94	0.88
Ang. Distortion	0.04	0.94	1	0.89
Lim. Tens. Strain	0.01	0.88	0.89	1

5.1. Generalisation of results from case study

In general, the choice of damage assessment method is more critical when the computed settlements are large. In particular, the correlation of total settlements with other parameters decreases the most with the severity of the scenario. Whilst the other parameters displayed a high correlation with each other, the total settlement displayed an exceptionally low correlation with all other damage parameters, and this decreased as the total settlements increased. This observation is most likely due to uniform settlements forming. This confirms the argument by Grant et al. (1974) that the correlation between total settlements and e.g. rotation would be low for higher total settlements. Furthermore, it was assumed that all variable relationships were monotonic, which was also confirmed graphically (Fig. 13), justifying the use of Spearman rank correlation.

The results also showed that the correlation for the maximum tensile strain (used for LTSM) against angular distortion and rotation is slightly lower than between angular distortion and rotation. This is most likely due to the relatively high complexity and variable dependency inherent in the maximum tensile strain, e.g. significant variations in deflection shapes due to the non-Gaussian distribution, and that the tilt is defined as the slope between the two intersection (wall edge) points. As such, the results suggest that rotation and angular distortion parameters would be enough for damage assessment at large areas, in line with the observations of Prosperi et al. (2023). Due to the large similarities in both definitions and results, angular distortion and rotation can be assumed equal (neglecting rigid body tilt), which is common in early-stage

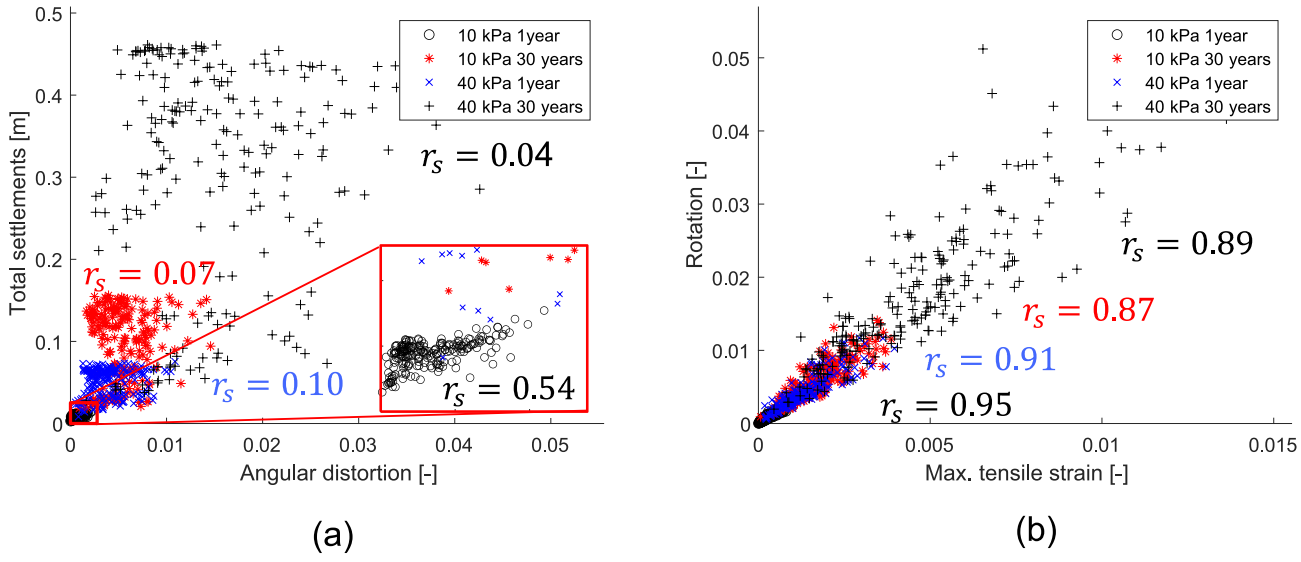

Fig. 13. Comparison of two damage parameters: (a) angular distortion vs. total settlements. (b) Maximum tensile strain vs. rotation.

Table 4
Contingency table for scenario 10kPa1y. Obs. = Observations, up = underpredictions, op = overpredictions.

Obs.	Model		
	A	B	C
A	25 %	30 %	31 %
B	45 %	58 %	46 %
C	31 %	13 %	23 %

$\chi^2 = 5.7, p = 0.22, up = 59\%, op = 11\%$

Table 5
Contingency table for scenario 10kPa30y. Obs. = Observations, up = underpredictions, op = overpredictions.

Obs.	Model		
	A	B	C
A	0 %	0 %	26 %
B	100 %	50 %	47 %
C	0 %	50 %	27 %

$\chi^2 = 2.0, p = 0.72, up = 1\%, op = 72\%$

Table 6
Contingency table for scenario 40kPa1y. Obs. = Observations, up = underpredictions, op = overpredictions.

Obs.	Model		
	A	B	C
A	17 %	29 %	26 %
B	67 %	36 %	47 %
C	17 %	36 %	27 %

$\chi^2 = 1.8, p = 0.78, up = 5\%, op = 68\%$

Table 7
Contingency table for scenario 40kPa30y. Obs. = Observations, up = underpredictions, op = overpredictions. NaN means no computed values in this validation class.

Obs.	Model		
	A	B	C
A	NaN	NaN	26 %
B	NaN	NaN	47 %
C	NaN	NaN	27 %

$\chi^2 = \mathrm{NaN}, p = \mathrm{NaN}, up = 0, op = 73\%$

assessments (see e.g. Son and Cording (2005)).

The chosen damage parameter was not found to be as important as the chosen limits for the damage criteria. This was seen especially in the comparison between Rankin (θ) and SOSM, where Rankin's criterion predicted significantly less damage than SOSM, despite the parameters being highly correlated. Since typology is unique for buildings (e.g. structural type, foundation type, geometry, number of openings etc.), different criteria may therefore apply to e.g. buildings in Gothenburg. It is, therefore, recommended that building typologies are identified and classified in the area where the analysis is carried out.

In general, the SOSM acted as the upper boundary and the Rankin (θ) acted as the lower boundary. Rankin (S) on the other hand fluctuated, most likely due to the forming of uniform settlements in scenarios where pore pressures had dissipated the most, e.g. 10 kPa drawdown with 30 years of consolidation. This is likely related to the choice of limiting values as discussed above.

5.2. Grid and resolution

The influence of resolution was analysed based on a decreased resolution (from 5 m to 10 m), as well as a sensitivity study performed on two of the settlement profiles from the metamodel. Although the building footprint was not considered in the latter case, the shape of the metamodel settlement troughs is assumed to represent model results with extremely fine resolution for a single building segment. This was performed in the absence of a finer hydro-stratigraphy. Nonetheless, both analyses indicated a positive trend between the resulting damage and grid resolution, highlighting the necessity of a sufficiently fine model resolution. The latter analysis also indicated that the magnitude and uncertainty of the total settlement parameter remained the same after a certain points-per-profile threshold (in this case 20–30), while rotation (and most likely angular distortion and deflection ratio) uncertainty and magnitude continued to increase. With the current resolution (5 m), a building with unrealistically long walls of 100–150 m should theoretically have accurate results even as resolution increases. In practice, however, the accuracy of chosen resolution should be determined by the resolution of the measured limit values from Table 1. Moreover, if soil-structure interaction is considered, the required resolution could be lower, as an increased building stiffness would decrease the rotation values. Nonetheless, the required grid resolution should be further studied to ensure conservative results.

The method currently only applies to profiles on constant x- and y-grids and does not consider the orientation of the walls. This is because the grid from the hydro-stratigraphic models was set up that way. There is therefore a risk of neglecting the most critical profile directions. However, if the building footprint is large enough, which increases the amount of settlement points, conservative results should still be assured in this preliminary assessment. Still, further development of the model to account for several orientations is recommended.

5.3. Validation and data availability

Finally, a validation was performed of the grid-based damage results using consultant vulnerability assessments based on prior damage protocols. In all scenarios, a large degree of under- and overpredictions could be found, meaning that existing damage most likely cannot be induced only by creep over the simulation period. Other causes of damage, e.g. longer periods of creep, historic loading and groundwater level changes as well as dynamic loading (from previous blasting of nearby rock or pile driving) are likely to have contributed to the observed damage. Moreover, current vulnerability assessments used only protocols prior to the underground construction.

To better describe what causes the under- and overpredictions, e.g. actual crack propagation and model errors, the validation needs to be complimented by another damage survey to better understand the crack propagation. Ideally, this would require a drawdown to occur and be sustained over a long period, which of course cannot be allowed. An alternative validation with detailed numerical analyses of a few buildings is recommended, simulating the actual pore pressure dissipation.

In addition to further damage surveys, borehole loggings, groundwater level- and settlement surveys would need to be performed at different locations, and not just in direct proximity to the tunnel. Standard oedometer and triaxial tests, performed on intact samples from multiple locations within 20 m depth are recommended. Strategically located bellow hoses or extensometers would furthermore complement the estimations of background creep with information about the compressibility in deeper clay layers.

5.4. Neglection of soil-structure interaction

The settlement and subsequent damage analysis performed in this

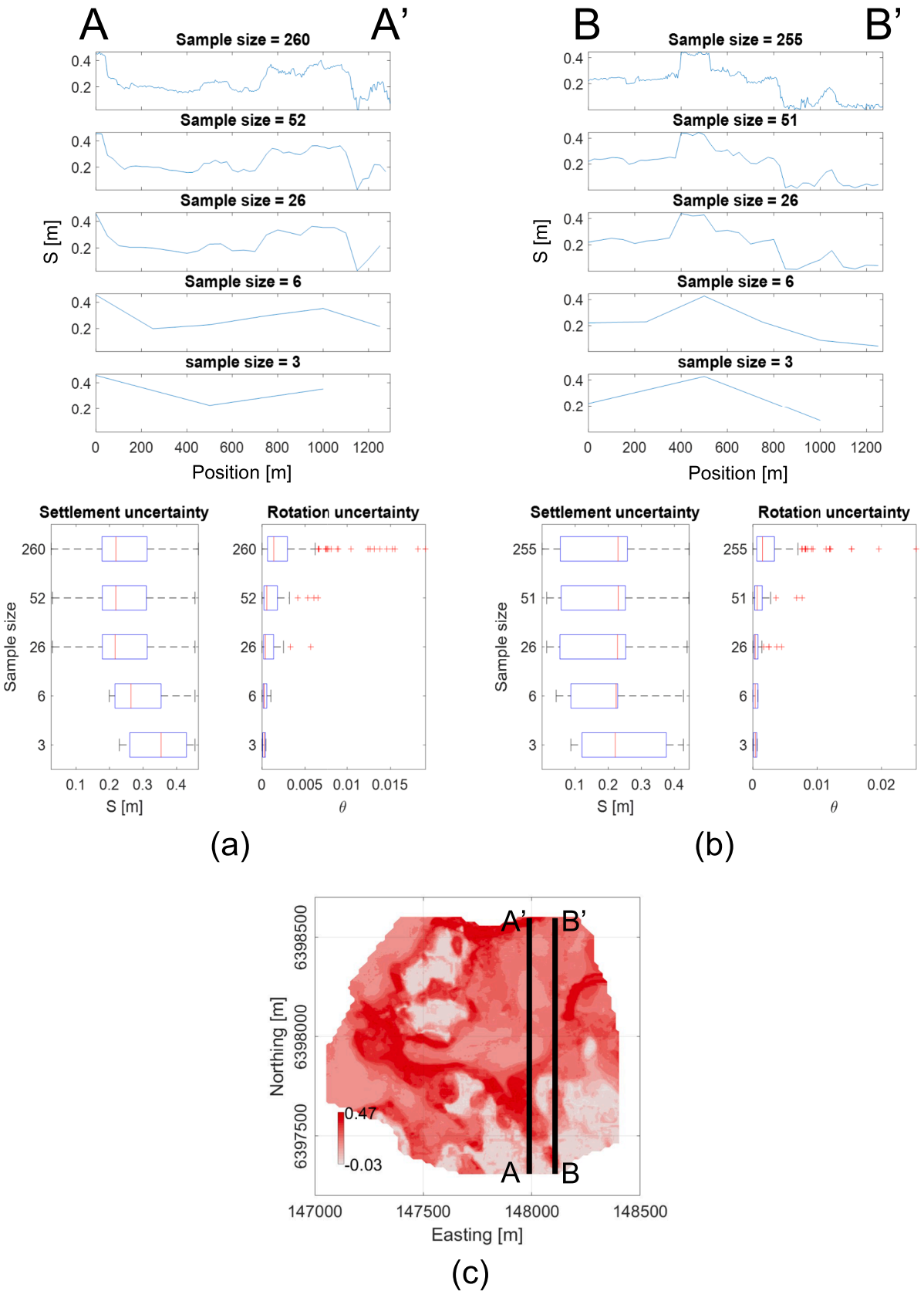

Fig. 14. Tests of different resolutions and their results span for settlements and rotation (a) profile A-A, (b) profile B-B. (c) Map of profiles.

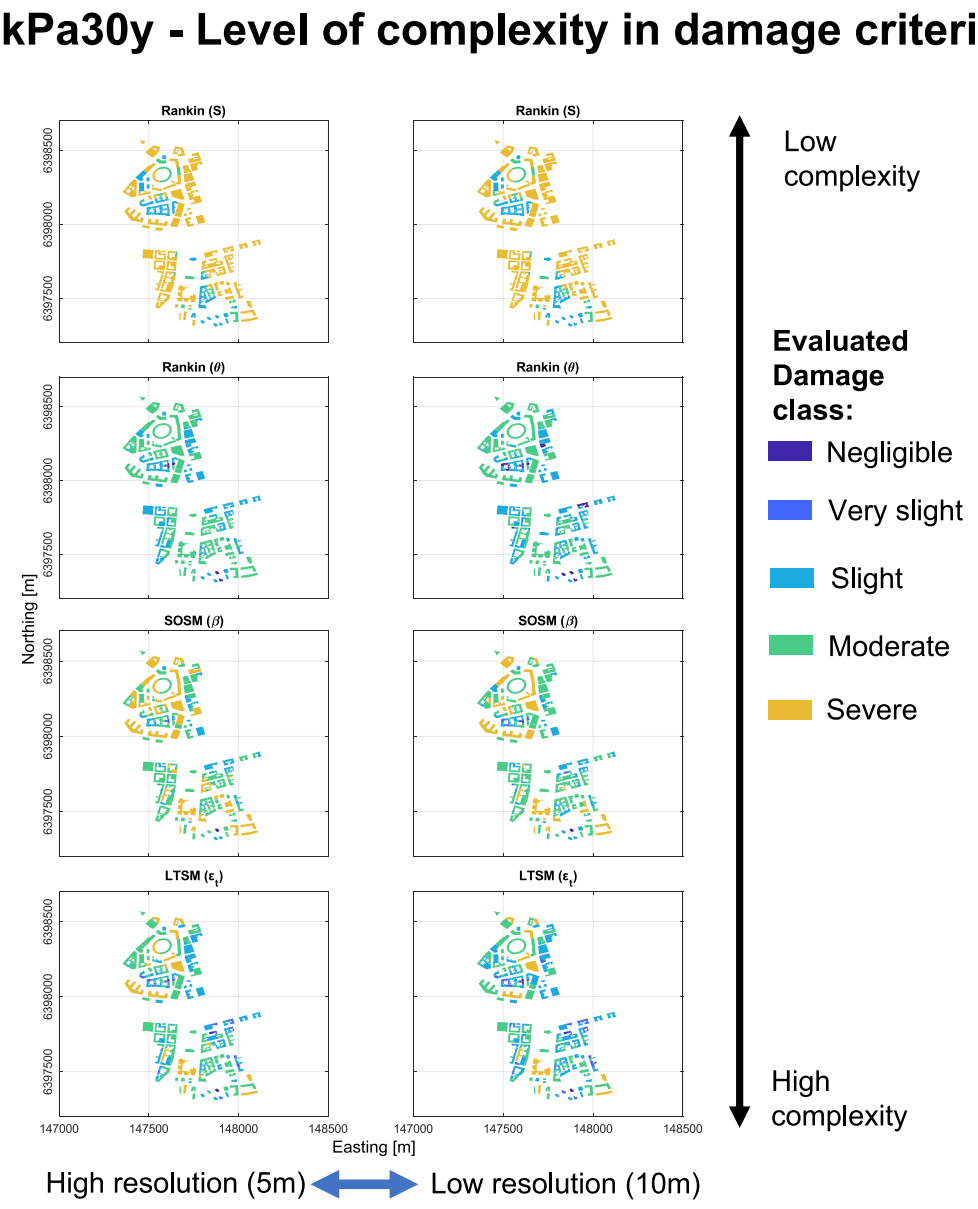

Fig. 15. Resulting damage using different resolutions. An example case of 10 kPa pore pressure drop 30 years consolidation. In the left and right columns, results from 5x5m and 10x10m resolution are displayed respectively.

paper have considered greenfield conditions. However, the influence of building and foundation stiffness on the settlement-related damage parameters can be significant. In urban environments, adjacent foundations would exert soil- and water-blocking effects on its surrounding soil movements and groundwater seepage during excavation dewatering (Xue et al., 2023; Zeng et al., 2023; Zeng et al., 2022a). This could limit or aggravate the dewatering-induced settlements.

Soil-structure interaction (SSI) is often studied through 3D numerical analyses, which is time-consuming and computationally demanding. The relative stiffness method (RSM) (Dimmock and Mair, 2008; Franzius et al., 2006; Potts and Addenbrooke, 1997; Son and Cording, 2005) has been extensively used to determine modification factors, the ratio between building and greenfield deformation. In this method, design charts are developed that describe the relationship between the relative building-soil stiffness and the modification factor. These design charts have been developed for various construction methods, structural types and soils. However, they do not only rely on stiffnesses but also on geometry and proximity to the excavation (volume loss, eccentricity, depth etc.). As far as we are aware, such approaches have only been applied in the cases of volume loss to tunnels and the settlement troughs of deep excavations. Thus, design charts for time-dependent groundwater drawdown-induced settlements have yet to be proposed. While building weight may increase the intensity of some of the damage parameters, the relative stiffness of the building and its foundation reduces it. As stiffness has a larger effect than weight, even without foundation effects (see e.g., Franzius (2003)), neglecting the relative stiffness, as done in this paper, most often leads to conservative results.

5.5. *Neglection of previous damage*

This study has focused on damage due to the direct impact of groundwater leakage to tunnels on subsidence, and thus any damage that the buildings might have had before the tunnel construction has been neglected. The modelling approach could also be used to investigate if any of the buildings are predicted to suffer damage in the long term from background creep only. It is also possible to extend the proposed method to account for the existing conditions of the building prior to construction, see e.g. Clarke and Laefer (2014) and Piciullo et al.

(2021). Such methods account for qualitative descriptions (shape, cultural value and initial condition) of the building but as a separate variable from the damage prediction. The overall risk can then be evaluated using a risk matrix with the severity of predicted damage on one axis and the vulnerability of the building on the other. However, considering initial damage is currently not possible with the data available.

5.6. Neglection of lateral strains

The effects of lateral strains on buildings are not directly considered, as the output from the metamodel is given as vertical settlements. However, as these vertical settlements emulate 2D hydro-mechanically coupled finite element analyses, the effect of lateral movements is implicitly considered. Moreover, the bellow hose measured absolute settlements which likely are higher than the purely vertical displacements. In the detailed analyses of the response of a building, lateral deformations can be important, and the proposed method should therefore be developed further to include the effect of deep-seated horizontal strains on individual buildings (in particular on those with mixed foundations and foundations with end bearing piles) that are considered to benefit from a more detailed assessment.

6. Conclusions

This research aimed to develop a building damage model which converts direct grid-based settlement results into damage parameters at the building scale, which can be used in early-stage damage assessments of underground projects or groundwater control considering large areas. The following main conclusions can be drawn:

For the first time, grid-based non-Gaussian settlement predictions were used as direct input into damage predictions for multiple buildings on a large area at the same time. It was shown that this method works for any type of 2D damage parameter, drawdown scenario and time at the scale adopted.

The sensitivity analyses showed that an increased grid resolution yielded more conservative results for rotation, and consequently, all damage parameters that stem from it, whereas accuracy for the total settlements was met even for relatively low resolutions. On the other hand, as other damage parameters increase with the number of points on a profile, predicted damage will be underestimated by a too-low resolution for such parameters. Therefore, with regards to likely compensation effects from neglecting e.g. building and foundation stiffness, the required grid resolution should be further studied to ensure conservative results.

Similarly, simplified profile orientation, not always aligned with walls, could potentially lead to unconservative results. Therefore, further development to account for several orientations is recommended for cities with irregular grids.

A validation of the model was performed; however, the cause of the observed pre-existing damage could not be determined using existing data. Therefore, validation against detailed numerical analyses or complementary damage observations of specifically chosen buildings is recommended.

When investigating the effect of the proposed method on 2D damage criteria, the choice of limiting values for a specific criterion was found to be more important than the type of parameter itself. The total settlement parameter showed the lowest correlation. Therefore, with respect to the complexity of the analyses and the correlation, parameters such as rotation and angular distortion are recommended.

The proposed methodology offers an automated solution for assessing non-Gaussian settlement-induced damage in large infrastructure projects at the start of the project. This enables the identification of locations where further investigations, and possible mitigation measures, are needed. The proposed method could be further developed to include effects of soil-structure interaction, previous damage as well as horizontal strains for the building and foundations considered most vulnerable. Finally, it is recommended that the limiting values for each damage criterion be based on the local building typology.

CRediT authorship contribution statement

Pierre Wikby: Writing – review & editing, Writing – original draft, Visualization, Validation, Software, Methodology, Investigation, Formal analysis, Data curation, Conceptualization. **Ezra Haaf:** Writing – review & editing, Validation, Supervision, Software, Project administration, Methodology, Investigation, Formal analysis, Data curation, Conceptualization. **Ayman Abed:** Writing – review & editing, Validation, Supervision, Software, Methodology, Investigation, Formal analysis, Data curation, Conceptualization. **Lars Rosen:** Writing – review & editing, Supervision, Resources, Project administration, Methodology, Funding acquisition, Conceptualization. **Jonas Sundell:** Writing – review & editing, Validation, Supervision, Software, Project administration, Methodology, Investigation, Funding acquisition, Formal analysis, Conceptualization. **Minna Karstunen:** Writing – review & editing, Supervision, Resources, Project administration, Methodology, Funding acquisition, Conceptualization.

Declaration of competing interest

The authors declare that they have no known competing financial interests or personal relationships that could have appeared to influence the work reported in this paper.

Data availability

Data will be made available on request.

Acknowledgements

The research presented is financed by the Swedish Transport Administration (Trafikverket), grant number TRV 2020/54637. The work is done as part of the Digital Twin Cities Centre supported by Sweden's Innovation Agency VINNOVA under Grant No. 2019-00041.

References

Agresti, A., Franklin, C., 2007. The art and science of learning from data. Upper Saddle River, New Jersey, p. 88.
Amavasai, A., Gras, J.-P., Sivasithamparam, N., Karstunen, M., Dijkstra, J., 2017. Towards consistent numerical analyses of embankments on soft soils. Eur. J. Environ. Civ. Eng. 26, 2616–2634.
Amavasai, A., Sivasithamparam, N., Dijkstra, J., Karstunen, M., 2018. Consistent Class A & C predictions of the Ballina test embankment. Computers and Geotechnics 93, 75–86.
Blanning, R.W., 1975. The construction and implementation of metamodels. Simulation 24, 177–184.
Boscardin, M.D., Cording, E.J., 1989. Building response to excavation-induced settlement. J. Geotech. Eng. 115, 1–21.
Bozkurt, S., Abed, A., Karstunen, M., 2023. Finite element analysis for a deep excavation in soft clay supported by lime-cement columns. Comput. Geotech. 162, 105687.
Broms, B.B., Fredriksson, A., Carlsson, L., 1977. Land subsidence in Sweden due to water-leakage into deep-lying tunnels and its effects on pile supported structures, Proceedings of the International Association of Hydrological Sciences, Anaheim.
Burbey, T.J., 2002. The influence of faults in basin-fill deposits on land subsidence, Las Vegas Valley, Nevada, USA. Hydrgeol. J. 10, 525–538.
Burland, J.B., Wroth, C., 1974. Settlement of buildings and associated damage, Proceedings of the British geotechnical society's conference on settlement of structures, Cambridge, pp. 611-654.
Burland, J.B., Broms, B.B., De Mello, V.F., 1977. Behaviour of foundations and structures. In: Proceedings of the 9th International Conference on Soil Mechanics and Foundation Engineering, pp. 495–546.
Burland, J.B., Mair, R.J., Standing, J.R., 2004. Ground performance and building response due to tunnelling, Advances in geotechnical engineering: The Skempton conference, pp. 291-342.
Clarke, J.A., Laefer, D.F., 2014. Evaluation of risk assessment procedures for buildings adjacent to tunnelling works. Tunn. Undergr. Space Technol. 40, 333–342.
Dalgic, K.D., Hendriks, M.A., Ilki, A., 2018. Building response to tunnelling-and excavation-induced ground movements: Using transfer functions to review the limiting tensile strain method. Struct. Infrastruct. Eng. 14, 766–779.

Dimmock, P.S., Mair, R.J., 2008. Effect of building stiffness on tunnelling-induced ground movement. Tunn. Undergr. Space Technol. 23, 438–450.
Drougkas, A., Verstrynge, E., Van Balen, K., Shimoni, M., Croonenborghs, T., Hayen, R., Declercq, P.-Y., 2020. Country-scale InSAR monitoring for settlement and uplift damage calculation in architectural heritage structures. Struct. Health Monit. 70, 108–122.
Fienen, M.N., Nolan, B.T., Kauffman, L.J., Feinstein, D.T., 2018. Metamodeling for groundwater age forecasting in the Lake Michigan basin. Water Resour. Res. 54, 4750–4766.
Franzius, J.N., Potts, D.M., Burland, J.B., 2006. The response of surface structures to tunnel construction. Proc. Inst. Civ. Eng. – Geotech. Eng. 159, 3-17.
Franzius, J.N., 2003. Behaviour of buildings due to tunnel induced subsidence, Civil and Environmental Engineering. Imperial College of Science, Technology and Medicine.
Furtney, J.K., Thielsen, C., Fu, W., Le Goc, R., 2022. Surrogate models in rock and soil mechanics: integrating numerical modeling and machine learning. Rock Mech. Rock Eng. 55, 2845–2859.
Giardina, G., Milillo, P., DeJong, M.J., Perissin, D., Milillo, G., 2019. Evaluation of InSAR monitoring data for post-tunnelling settlement damage assessment. Struct. Control Health Monit. 26, 1–19.
Gokhale, D.V., Kullback, S., 1978. The Information in Contingency Tables.
Grant, R., Christian, J.T., Vanmarcke, E.H., 1974. Differential settlement of buildings. J. Geotech. Eng. Div. 100, 973–991.
Gras, J.-P., Sivasithamparam, N., Karstunen, M., Dijkstra, J., 2017. Strategy for consistent model parameter calibration for soft soils using multi-objective optimisation. Comput. Geotech. 90, 164–175.
Gras, J.-P., Sivasithamparam, N., Karstunen, M., Dijkstra, J., 2018. Permissible range of model parameters for natural fine-grained materials. Acta Geotechnica 13, 387–398.
Hsieh, P.-G., Ou, C.-Y., 1998. Shape of ground surface settlement profiles caused by excavation. Can. Geotech. J. 35, 1004–1017.
Kang, F., Li, J.-S., Wang, Y., Li, J., 2017. Extreme learning machine-based surrogate model for analyzing system reliability of soil slopes. Eur. J. Environ. Civ. Eng. 21, 1341–1362.
Korff, M., 2013. Response of piled buildings to the construction of deep excavations. IOS Press.
Langford, J., Baardvik, G., Karlsrud, K., 2016. Pore pressure reduction and settlements induced by deep supported excavations in soft clay. Proceedings of the 17th Nordic Geotechnical Meeting.
Mahmoudpour, M., Khamehchiyan, M., Nikudel, M.R., Ghassemi, M.R., 2016. Numerical simulation and prediction of regional land subsidence caused by groundwater exploitation in the southwest plain of Tehran, Iran. Eng. Geol. 201, 6–28.
Mair, R., Taylor, R., Burland, J., 1996. Prediction of ground movements and assessment of risk of building damage due to bored tunnelling. Geotechnical Aspects of Underground Construction in Soft Ground 713–718.
Merisalu, J., Sundell, J., Rosén, L., 2023. Probabilistic cost-benefit analysis for mitigating hydrogeological risks in underground construction. Tunn. Undergr. Space Technol. 131, 104815.
Ninić, J., Meschke, G., 2015. Model update and real-time steering of tunnel boring machines using simulation-based meta models. Tunn. Undergr. Space Technol. 45, 138–152.
Obel, M., Ahrens, M.A., Mark, P., 2020. Metamodel-based prediction of structural damages due to tunneling-induced settlements. ASCE-ASME J. Risk Uncertainty Eng. Syst., Part A: Civ. Eng. 6, 04020044.
Peduto, D., Nicodemo, G., Maccabiani, J., Ferlisi, S., 2017. Multi-scale analysis of settlement-induced building damage using damage surveys and DInSAR data: A case study in The Netherlands. Eng. Geol. 218, 117–133.
Peduto, D., Korff, M., Nicodemo, G., Marchese, A., Ferlisi, S., 2019. Empirical fragility curves for settlement-affected buildings: Analysis of different intensity parameters for seven hundred masonry buildings in The Netherlands. Soils Found. 59, 380–397.
Peduto, D., Prosperi, A., Nicodemo, G., Korff, M., 2021. District-scale numerical analysis of settlements related to groundwater lowering in variable soil conditions. Can. Geotech. J. 59, 978–993.
Piciullo, L., Ritter, S., Lysdahl, A.O.K., Langford, J., Nadim, F., 2021. Assessment of building damage due to excavation-induced displacements: The GIBV method. Tunn. Undergr. Space Technol. 108, 103673.
Polshin, D.E., Tokar, R., 1957. Maximum allowable non-uniform settlement of structures, Proc., 4th Int. Conf. on Soil Mechanics and Foundation Engineering. Butterworth's, London, pp. 402-405.
Potts, D.M., Addenbrooke, T.I., 1997. A structure's influence on tunnelling-induced ground movements. Proceedings of the Institution of Civil Engineers - Geotechnical Engineering 125, 109-125.
Prosperi, A., Korswagen, P.A., Korff, M., Schipper, R., Rots, J.G., 2023. Empirical fragility and ROC curves for masonry buildings subjected to settlements. J. Build. Eng. 68, 106094.
Rankin, W.J., 1988. Ground movements resulting from urban tunnelling: predictions and effects. Geol. Soc., London, Eng. Geol. Special Publications 5, 79–92.
Shen, S.-L., Xu, Y.-S., 2011. Numerical evaluation of land subsidence induced by groundwater pumping in Shanghai. Can. Geotech. J. 48, 1378–1392.
Sivasithamparam, N., Karstunen, M., Bonnier, P., 2015. Modelling creep behaviour of anisotropic soft soils. Comput. Geotech. 69, 46–57.
Skempton, A.W., MacDonald, D.H., 1956. The allowable settlements of buildings. Inst. Civ. Eng. 5, 727–784.
Son, M., Cording, E.J., 2005. Estimation of building damage due to excavation-induced ground movements. J. Geotech. Geoenviron. Eng. 131, 162–177.
Sundell, J., Rosén, L., Norberg, T., Haaf, E., 2016. A probabilistic approach to soil layer and bedrock-level modeling for risk assessment of groundwater drawdown induced land subsidence. Eng. Geol. 203, 126–139.
Sundell, J., Haaf, E., Tornborg, J., Rosén, L., 2019. Comprehensive risk assessment of groundwater drawdown induced subsidence. Stoch. Env. Res. Risk A. 33, 427–449.
Teatini, P., Ferronato, M., Gambolati, G., Gonella, M., 2006. Groundwater pumping and land subsidence in the Emilia-Romagna coastland, Italy. Modeling the past Occurrence and the Future Trend. Water Resources Research 42.
Tornborg, J., Karlsson, M., Kullingsjö, A., Karstunen, M., 2021. Modelling the construction and long-term response of Göta Tunnel. Comput. Geotech. 134, 104027.
Tornborg, J., Karlsson, M., Karstunen, M., 2023. Permanent sheet pile wall in soft sensitive clay. J. Geotech. Geoenviron. Eng. 149, 05023003.
Trafikverket, 2014. PM F - 001 PM Inventering tidigare utförda hydrogeologiska undersökningar, pp. 1-79.
TreMaps, 2022. Gothenburg TSX Vertical displacement rates November.
Wang, Q., Fang, H., Shen, L., 2016. Reliability analysis of tunnels using a metamodeling technique based on augmented radial basis functions. Tunn. Undergr. Space Technol. 56, 45–53.
Wikby, P., Abed, A., Karlsson, M., Sundell, J., Karstunen, M., 2023. The influence of parameter variability on subsidence. In: Zdravkovic, L., Kontoe, S., Taborda, D., Tsiampousi, A. (Eds.), 10th European Conference on Numerical Methods in Geotechnical Engineering. London.
Xue, T., Xue, X., Long, S., Chen, Q., Lu, S., Zeng, C., 2023. Effect of pre-existing underground structures on groundwater flow and strata movement induced by dewatering and excavation. Water 15, 814.
Ye, S., Xue, Y., Wu, J., Yan, X., Yu, J., 2016. Progression and mitigation of land subsidence in China. Hydrgeol. J. 24, 685.
Zeng, C.-F., Zheng, G., Xue, X.-L., 2019. Responses of deep soil layers to combined recharge in a leaky aquifer. Eng. Geol. 260, 105263.
Zeng, C.-F., Wang, S., Xue, X.-L., Zheng, G., Mei, G.-X., 2021. Evolution of deep ground settlement subject to groundwater drawdown during dewatering in a multi-layered aquifer-aquitard system: Insights from numerical modelling. J. Hydrol. 603, 127078.
Zeng, C.-F., Liao, H., Xue, X.-L., Long, S.-C., Luo, G.-J., Diao, Y., Li, M.-G., 2022a. Responses of groundwater and soil to dewatering considering the barrier effect of adjacent metro station on multi-aquifers. J. Hydrol. 612, 128117.
Zeng, C.-F., Wang, S., Xue, X.-L., Zheng, G., Mei, G.-X., 2022b. Characteristics of ground settlement due to combined actions of groundwater drawdown and enclosure wall movement. Acta Geotech. 17, 4095–4112.
Zeng, C.-F., Chen, H.-B., Liao, H., Xue, X.-L., Chen, Q.-N., Diao, Y., 2023. Behaviours of groundwater and strata during dewatering of large-scale excavations with a nearby underground barrier. J. Hydrol. 620, 129400.
Zheng, G., Ha, D., Zeng, C., Cheng, X., Zhou, H., Cao, J., 2019. Influence of the opening timing of recharge wells on settlement caused by dewatering in excavations. J. Hydrol. 573, 534–545.